Molecular Catalysis xxx (xxxx) xxxx

Contents lists available at ScienceDirect

Molecular Catalysis

journal homepage: www.elsevier.com/locate/mcat

The effect of support properties on n-octanol oxidation performed on gold – silver catalysts supported on MgO, ZnO and Nb_2O_5

Iveta Kaskow[a,b], Izabela Sobczak[a,*], Maria Ziolek[a], Vicente Cortés Corberán[b,*]

[a] Adam Mickiewicz University in Poznan, Faculty of Chemistry, Uniwersytetu Poznańskiego 8, 61-614 Poznan, Poland
[b] Institute of Catalysis and Petroleumchemistry (ICP), CSIC, Marie Curie 2, 28049 Madrid, Spain

ARTICLE INFO

Keywords:
MgO
ZnO and Nb_2O_5 supports
Au-Ag loading
Redox
Acid-base properties
Electronegativity
n-octanol oxidation

ABSTRACT

Catalytic behaviour of supported nanometal catalysts for alcohols selective oxidation depends on the nature of the support and its surface. To identify the main feature that could explain these effects, supported mono- (Au) and bimetallic (AuAg) catalysts were prepared by using pure MgO, ZnO and Nb_2O_5, representative of three different types of oxides (basic, amphoteric and acidic, respectively), to get homogeneous metal-support interaction for each catalyst. The catalysts were characterized by XRD, N_2 physisorption, TEM, UV–vis, XPS and 2-propanol decomposition as test reaction. It was found that the catalytic activity is influenced by the electron mobility between the gold nanoparticles and the support, which in turns depends on the intermediate electronegativity of the support. Selectivity in n-octanol oxidation was determined by redox properties of the gold species, the acid-base properties of the supports and the catalyst pretreatment. Silver addition modified the acid-base properties of the catalytic system, thus influencing the selectivity in n-octanol oxidation. Pretreatment of the catalyst (drying in air or thermal treatment in hydrogen flow) had a significant impact on its activity and selectivity.

1. Introduction

Bimetallic catalysts usually exhibit better catalytic properties than their monometallic equivalents. This is caused by the so-called synergistic effect of mutual interactions between two metals. Among various systems studied, bimetallic gold catalysts (Au-Cu, Au-Pd, Au-Pt, Au-Ag, etc.) are nowadays in the centre of research interest. They are active in various reactions like the water gas shift reaction (WGSR), hydrogenation of organic compounds, synthesis of hydrogen peroxide, low temperature oxidation of CO or oxidation of alcohols such as methanol, ethanol, glycerol, benzyl alcohol or n-octanol [e.g. 1–10].

Selective oxidation of alcohols plays a key role in industry [7]. Many valuable chemicals as aldehydes, esters and acids can be synthesized from them. More than 100 million tons of carbonyl compounds are produced yearly by alcohol oxidation. The disadvantage of this reaction is the use of stoichiometric amounts of expensive and toxic oxidizing agents (transition metal oxides and their salts or compounds containing halogens). That is why there is an urgent need to develop processes with the use of heterogeneous catalysts and oxygen as a cheap and non-toxic alternative to toxic oxidants [6,10–16].

n-Octanol belongs to the group of low fatty alcohols. It is known that the gold-containing catalysts show high catalytic activity and selectivity in aerobic oxidation of long-chain alcohols performed in the liquid-phase and under mild conditions such as low reaction temperatures (below 413 K) and atmospheric pressure [e.g. 6,7,10,11]. Both, mono- and bimetallic gold and/or silver catalysts have been studied in catalytic n-octanol oxidation in the liquid phase in the absence of a base. Haruta's group has studied Au/NiO and Au/CeO_2 catalysts [8] and found that the choice of a suitable support for gold nanoparticles enabled direct oxidation of unreactive n-octanol to octanoic acid and octyl octanoate in the absence of a base. Au/NiO exhibited excellent selectivity to octanoic acid (97% in H_2O/dioxane solvent) at full conversion (373 K, 18 h, 0.5 MPa O_2). In contrast, Au/CeO_2 selectively produced octyl octanoate as a major product, with a 70% selectivity and 90% alcohol conversion. TiO_2 has been studied as a support for gold and gold - silver nanocatalysts [6,10]. For monometallic materials it has been shown [6] that the addition of magnesium onto the support ($Au/Mg/TiO_2$) improved the catalytic activity of Au/TiO_2. On the contrary, iron deposited on TiO_2 caused a decrease in the Au/TiO_2 activity. It has been explained by electron-donor properties of magnesium oxide and electron-acceptor properties of iron oxide. The addition of MgO created balance between intermediate oxidation states of gold on the surface of Mg/TiO_2 support that was responsible for the high catalytic activity of $Au/Mg/TiO_2$. The same trend has been observed for

* Corresponding authors.
E-mail addresses: sobiza@amu.edu.pl (I. Sobczak), vcortes@icp.csic.es (V.C. Corberán).

https://doi.org/10.1016/j.mcat.2019.110674
Received 5 July 2019; Received in revised form 14 October 2019; Accepted 14 October 2019

bimetallic catalysts [10]. The activity of bimetallic AuAg/TiO_2 samples increased as a result of modification of the support with donor additives (La, Mg), while acceptor additives (Ce, Fe) decreased it. Moreover, it has been proved that the presence of La in the support inhibits the formation of Au-Ag alloy. Thanks to the stabilization of the active centres in their optimal electronic state, the high activity and stability of AuAg/La/TiO_2 catalyst in n-octanol oxidation was obtained.

The aim of this work was to identify the main common feature that could explain all these observed effects of the support nature and the preactivation conditions on the surface and catalytic properties of nanometal catalysts for n-octanol oxidation in the liquid phase under mild conditions, and more specifically of bimetallic AuAg catalysts. To attain that goal, at a variance of previously published papers focused on the surface modification of one specific support, in this paper we investigated three very different single oxide supports, looking for an homogeneous metal-support interaction for each catalyst.

Thus, three metal oxides (MgO, ZnO and Nb_2O_5), representative of different types (basic, amphoteric and acidic, respectively), were used in the present work as model supports for gold and silver to evaluate the role of surface properties of the supports on the effectiveness of gold-silver catalysts in n-octanol oxidation with oxygen.

2. Experimental

2.1. Catalysts preparation

2.1.1. Materials

The chemical compounds used in this study are: magnesium oxide (Aldrich, ≥ 99%), niobium pentoxide (hydrated, CBMM-Brazil), pluronic P123 ((poly(ethylene glycol)-block-poly(propylene glycol)-block-poly-(ethylene glycol)-block), zinc acetate (anhydrous, Aldrich, > 99.0%), oxalic acid (Aldrich, > 99,999%), distilled water, methanol, (3-aminopropyl)trimethoxysilane (APTMS, Aldrich, 95%), dry toluene (POCH, ≥99.8%), sodium borohydride ($NaBH_4$, Aldrich, ≥98%), chloroauric acid ($HAuCl_4 \cdot 4H_2O$, Aldrich, 99,995%) and silver nitrate ($AgNO_3$, Aldrich, ≥99%). The chemicals were not purified before use.

2.1.2. Zinc oxide synthesis

Zinc oxide was synthesized by the method described in [17]. Firstly, pluronic P123 (8.6 g) was dissolved in methanol (83 mL) and zinc acetate (10 g) in distilled water (83 mL). These two solutions were mixed together on a magnetic stirrer for one hour. Meanwhile a solution of acetic acid (4.9 g) in water-methanol (83 mL of H_2O, 83 mL of MeOH) was prepared and slowly added dropwise to the mixture of zinc acetate and pluronic P123 upon stirring. The white precipitate formed was filtered and washed with water and methanol. The solid obtained was dried at 333 K and calcined in 723 K for 4 h to get the final product.

2.1.3. Functionalization of the supports (ZnO, MgO, Nb_2O_5) with APTMS

The three oxides were grafted with (3-aminopropyl)trimethoxysilane to functionalize the supports. Eight grams of ZnO, MgO or Nb_2O_5 were heated at 383 K with a mixture of dry toluene (200 mL) and APTMS (20 mL) under reflux for 18 h. Then, the solid was recovered by filtration and washing with toluene (200 mL), water (100 mL) and acetonitrile (100 mL). The last step was drying of the solid at 353 K.

2.1.4. Metal incorporation

To get monometallic catalysts, adequate amount of the support was mixed with a water solution of gold or silver precursor ($HAuCl_4$ or $AgNO_3$, in amounts needed to get a final content of 2 wt. % of Au or Ag) for one hour at room temperature. Then it was filtered and washed with water. The obtained solid was mixed with the water solution of sodium borohydrate ($NaBH_4$) for 20 min and then filtered again. To obtain the bimetallic AuAg catalyst the second step was stirring of the gold containing material with the water solution of silver precursor ($AgNO_3$, as needed to get a final 1 wt. % of Ag). The final materials were obtained by drying at 373 K and calcination at 773 K (MgO and ZnO based catalysts) or at 673 K (Nb_2O_5 supported catalysts) for 4 h

2.2. Characterization of the materials

The XRD patterns of the supports and calcined catalysts were obtained on a D8 Advance diffractometer (Bruker) using CuK_α radiation ($\lambda = 0.154$ nm), with a step size of 0.05° in the $2\Theta = 6 - 60°$ range.

The N_2 adsorption/desorption isotherms were obtained at 77 K using a Micromeritics ASAP 2020 Physisorption Analyzer. The samples were pre-treated in situ under vacuum at 573 K. The surface area was calculated by the BET method, whereas the pore volume and the diameter were estimated according to BJH method from the adsorption branch of the isotherm.

The actual metal loadings in the samples were measured by inductively coupled plasma atomic emission spectroscopy (ICP-OES) with a Perkin Elmer ICP-OES Optima 3300 DV spectrometer.

UV-vis spectra of the catalysts calcined and pre-treated in hydrogen flow (samples denoted with the suffix –H) were recorded using a Varian-Cary 300 Scan UV–vis spectrophotometer. Powdered samples were placed in a cell equipped with a quartz window. The spectra were recorded in the range from 800 to 190 nm (the wavelength resolution was 0.4 nm). Spectralon was used as a reference material.

X-ray photoelectron spectroscopy (XPS) was performed in a SPECS (Germany) photoelectron spectrometer equipped with a monochromatic microfocused Al K X-ray source (1486.6 eV). The binding energy of gold species in monometallic samples were corrected to C1s, with the known binding energy of 284.6 eV.

For transmission electron microscopy (TEM) measurements a JEOL 2000 electron microscope operating at 80 kV was used. The materials calcined and pre-treated in hydrogen flow (samples denoted with the suffix –H) were deposited on a carbon-coated grid and transferred to the above-mentioned microscope. The sizes of metal crystallites were estimated from TEM images by measuring about 100 particles on the images and plotting crystallite sizes distribution. The standard deviation of these measurements was calculated from the formula:

$S = [\Sigma\ (d_i - d_{av})^2 / \Sigma\ n_i]^{1/2}$, where: n_i – number of crystallites measured, d_i – size of the indicated crystallite, d_{av} – mean crystallite size.

The conversion (dehydration and dehydrogenation) of 2-propanol (POCH) was performed in a microcatalytic pulse reactor inserted between the sample inlet and the column of an SRI 310C chromatograph. The catalyst bed (0.1 g with a grain size fraction of $0.5 < Ø < 1$ mm) was first activated at 673 K for 2 h under nitrogen flow (40 $cm^3\ min^{-1}$). The 2-propanol conversion was studied at 473, 523 and 573 K using 3 µl pulses of alcohol under nitrogen flow (40 $cm^3\ min^{-1}$). The reactant and reaction products: propene, 2-propanone (acetone) and diisopropyl ether were analysed using a SRI 310C gas chromatograph on line with microreactor. The reaction mixture was analysed on 2 m column filled with Carbowax 400 loaded on Chromosorb W in nitrogen flow (40 $cm^3\ min^{-1}$) and detected by FID.

2.3. Oxidation of n-octanol

Prior to testing the reaction of n-octanol (Merck, 99%, HPLC grade) oxidation, the calcined catalysts were either dried overnight at 393 K (denoted as -D) or reduced in 10 mL/min of H_2 for 1 h in 673 K (denoted as -H). The appropriate amount of pre-treated catalyst (Au/n-octanol = 100 mol/mol) was put into a four-necked round bottom flask and 25 mL of 0.1 M n-octanol solution in n-heptane (Scharlau, 99%, HPLC grade) was added. The flask was equipped with a thermocouple, oxygen inlet and septum cap. The reaction was run for 6 h at 353 K under reflux, upon continuous stirring, while O_2 (Air Liquide, 99.99%) was bubbled through the reaction mixture. Small amounts of the reaction mixture were collected at specified run times during the oxidation process (0.5, 1, 2, 4 and 6 h) to analyse the progress of the reaction. The

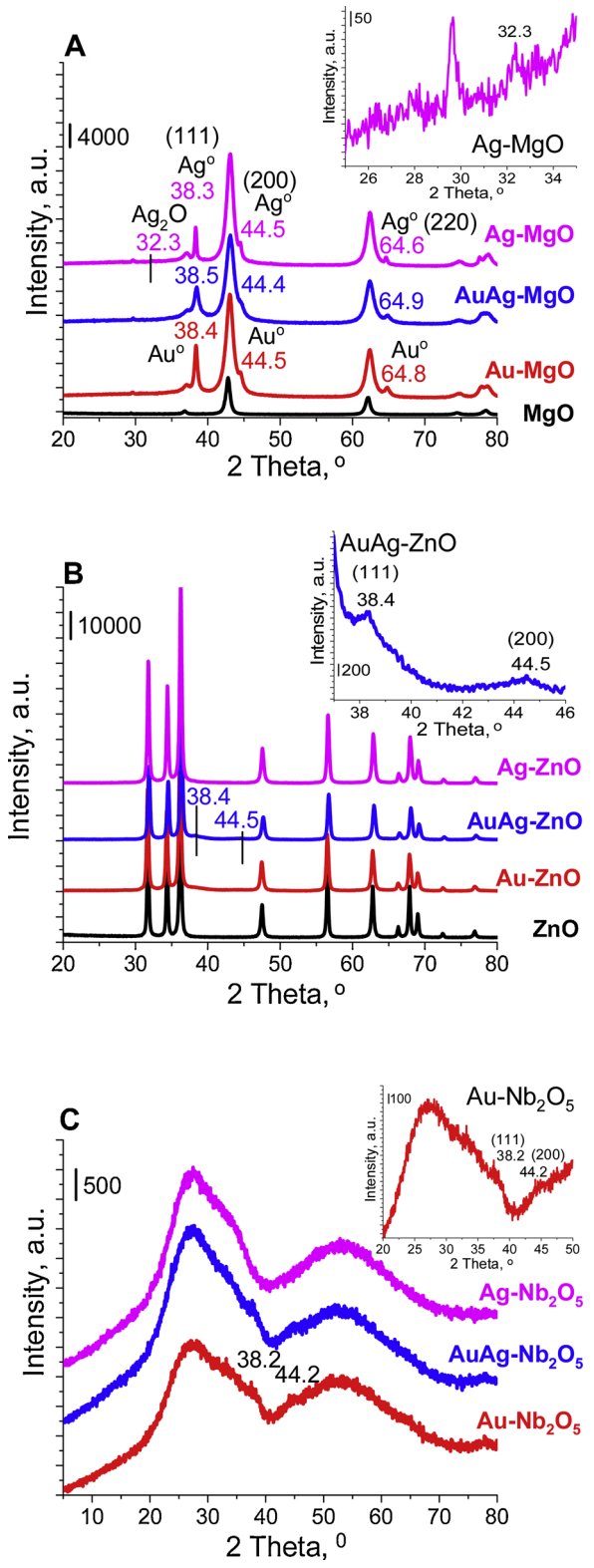

Fig. 1. X-Ray diffractograms of metal oxides before and after noble metals deposition: MgO (A), ZnO (B) and Nb_2O_5 (C).

catalyst was separated from these samples using nylon syringe filters (pore 0.45 µm) to analyse the reaction products on Varian 450 gas chromatograph equipped with a capillary DB wax column (15 m × 0.548 mm) and FID. Helium was used as a carrier gas.

3. Results and discussion

Gold, silver or gold and silver were supported on MgO, ZnO and Nb_2O_5, as models of different types of oxides (basic, amphoteric and acidic, respectively), to obtain three groups of catalysts with different surface properties to be applied for n-octanol oxidation.

3.1. Structure/texture characterization - XRD and N_2 physisorption studies

X-Ray diffraction patterns of MgO, ZnO and Nb_2O_5 supports are shown in Fig. 1. The patterns of MgO and ZnO (Fig. 1A, B) indicate the crystalline structure of both oxides. The pattern of magnesium oxide was fitted to the cubic structure of MgO (JCPDS card No. 75-1525), with the main peaks at 2θ = 37.0°, 42.8°, 62.2°, 74.4°, 78.4°. The pattern of zinc oxide, with the characteristic peaks at 2θ = 31.8°, 34.4°, 36.2°, 47.5°, 56.6° corresponding to the (100), (002), (101), (102), (110) planes, was assigned to the hexagonal zincite structure of ZnO (JCPDS card No.01-089-1397). The incorporation of gold, silver or gold and silver to both crystalline supports followed by calcination did not cause any significant changes in the diffractograms. The XRD pattern of niobia (Fig. 1C) reveals amorphous features of this support. No significant differences can be observed between the diffractograms of the support and the corresponding supported catalysts.

The textural data calculated from low temperature nitrogen adsorption are shown in Table 1. The BET surface areas of MgO and Nb_2O_5 are relatively large (above 100 m^2/g), whereas ZnO shows a much smaller one (16 m^2/g). While the BET surface area of Nb_2O_5 significantly decreased after incorporation of the metals, for MgO an increase in the surface area was observed, whereas for ZnO this parameter did not change. The changes in porosity were observed only for niobia by an increase in pore diameter. The loading of metals in pores of Nb_2O_5 caused a decrease in surface area. Its pore size distribution (Fig. S1) indicated that niobia contained not only mesopores but also micropores. The latter disappeared upon noble metals loading (i.e. they became clogged up by metal deposits). This causes the decrease in BET surface area upon introduction of metals. In MgO, the incorporation of noble metals generated additional porosity as shown in Fig. S2, which resulted in the growth of surface area. In contrast, the textural parameters of ZnO were almost untouched after incorporation of metals.

3.2. Metals content

Table 2 presents the metal loadings of the catalysts. It is clear that gold loading in mono- and bimetallic materials was equal or close to the

Table 1
Textural parameters of supports and catalysts calculated from nitrogen adsorption isotherms.

Catalyst	BET, m^2/g	Pore volume, BJH, cm^3/g	Average pore diameter, BJH, nm
MgO	144	0.50	16
Au-MgO	170	0.50	12
AuAg-MgO	172	0.50	12
Ag-MgO	156	0.50	13
ZnO	16	0.16	35
Au-ZnO	17	0.15	34
AuAg-ZnO	16	0.18	37
Ag-ZnO	16	0.15	38
Nb_2O_5	111	0.12	4
Au-Nb_2O_5	52	0.08	6
AuAg-Nb_2O_5	64	0.10	6

Table 2
Metal loading and size of metal crystallites of the catalysts.

Catalyst	Au, wt. % nominal	Au, wt. % real	Ag, wt. % nominal	Ag, wt. % real	Au/Ag real	Average metal crystallite size, nm
u-MgO	2.0	1.7	-	-	-	16.9 ± 5.0
uAg-MgO	2.0	1.8	1.0	0.6	1.6	8.9 ± 4.5
g-MgO	-	-	2.0	1.1	-	-
u-ZnO	2.0	1.9	-	-	-	2.6 ± 0.8
uAg-ZnO	2.0	2.0	1.0	1.0	1.1	3.8 ± 1.1
g-ZnO	-	-	2.0	0.9	-	-
u-Nb_2O_5	2.0	1.8	-	-	-	5.3 ± 2.3
AuAg-Nb_2O_5	2.0	1.9	1.0	0.8	1.3	3.7 ± 1.3
Ag-Nb_2O_5	-	-	2.0	1.4	-	-

nominal one. It showed that the modification using grafting with APTMS was effective for gold incorporation under the conditions used in this work. Silver cations interacted with negatively charged metallic gold, formed during the preparation procedure as a result of reduction with $NaBH_4$ [18], but the actual loading of silver depended on the type of support. For bimetallic samples based on ZnO and Nb_2O_5 it was equal or close to the nominal one, whereas for AuAg-MgO the real metal loading was lower than the nominal one. When monometallic silver samples were prepared, the amount of silver was much lower than the nominal (ca. 50% of efficiency) due to the electrostatic repulsion between Ag^+ and NH_3^+ ions (in protonated APTMS).

3.3. Acid-base properties of the supports and catalysts: 2-propanol decomposition

The acid-base properties of the support can play an important role in the performance of catalysts in n-octanol oxidation. The products distribution is an indicator of acid-basic-redox properties of the catalyst surface (propene is formed on acidic sites, acetone on basic/redox centres, whereas diisopropyl ether on pairs of Lewis acid-base centres - Scheme S1) [19].

The results shown in Table 3 indicate that 2-propanol conversion depended on the nature of the support. From among the metal oxides used as supports, the highest conversion of 2-propanol was observed on niobia, the main reaction product being propene. Both features indicated the acidic properties of this support. Moreover, a small amount of diisopropyl ether was detected in the reaction products indicating the presence of Lewis acid-base pairs. Activities of MgO and ZnO were much lower and comparable. The observed 100% selectivity to acetone obtained on MgO proved the basic properties of this support. For ZnO, at the lower reaction temperatures (473, 523 K), acetone was predominant among the reaction products, indicating the presence of basic centres. At 573 K acetone and propene were detected (58% and 41% selectivity, respectively) confirming acid-base features of zinc oxide. Incorporation of silver to the support did not change significantly the properties of the catalyst at the lower reaction temperature: the activity and selectivity were very similar to those without silver. However, an increase in the basic properties of the catalyst can be concluded from the increase in the acetone selectivity at 573 K (in comparison to that of ZnO).

Incorporation of gold species to ZnO and MgO increased the alcohol conversion and changed the acidic-basic properties on both supports, but not in the same direction. In the case of Au-ZnO acetone selectivity increased, evidencing the increase in basicity, whereas for Au-MgO the basicity from the support decreased. The selectivity to acetone decreased and some amounts of propene and ether appeared, indicating the formation of acidic sites as a result of gold introduction from chloroauric acid. Gold incorporation to the acidic support (Nb_2O_5) gave lower conversion of alcohol, a decrease in the products formed on acidic sites and an increase in acetone formation. It means that acid centres present on the support became covered by the metal loaded.

Table 3
Decomposition of 2-propanol on supports and catalysts.

Catalyst	Temp., K	Conversion, %	Selectivity, %		
			Acetone	Propene	Ether
MgO	473	1	100	0	0
	523	3	100	0	0
	573	15	100	0	0
ZnO	473	3	99	1	0
	523	2	96	4	0
	573	12	58	41	1
Nb_2O_5	473	49	0	97	3
	523	75	0	99	1
	573	90	0	95	5
Ag-ZnO	473	2	99	1	0
	523	3	99	1	0
	573	13	70	30	0
Au-ZnO	473	6	100	0	0
	523	12	99	1	traces
	573	30	85	4	11
AuAg-ZnO	473	4	62	32	6
	523	16	44	38	18
	573	37	40	50	10
Au-MgO	473	6	67	10	23
	523	11	93	6	1
	573	18	87	12	1
Au-MgO-H	473	8	80	11	9
	523	14	82	18	traces
	573	22	67	33	traces
AuAg-MgO	473	18	96	4	traces
	523	28	97	3	traces
	573	39	97	3	traces
AuAg-MgO-H	473	17	94	4	2
	523	31	88	8	4
	573	44	70	19	11
Au-Nb_2O_5	473	19	28	15	57
	523	43	9	46	45
	573	48	5	79	16
AuAg-Nb_2O_5	473	25	17	15	68
	523	50	4	64	32
	573	55	3	89	8

The addition of silver to gold containing samples increased the catalyst activity in 2-propanol decomposition. The highest increase was observed for AuAg-MgO. It is important to note the changes in selectivity caused by silver addition. The addition of Ag to Au supported on ZnO and Nb_2O_5 decreased the acetone selectivity and increased propene formation. Thus, one can conclude about the increase in acidity upon silver incorporation. A different sequence of changes in acidic-basic properties was observed for AuAg-MgO. After addition of silver to Au-MgO, basic sites became restored on AuAg-MgO (acetone selectivity increased in comparison to that of Au-MgO). The activity of AuAg-MgO treated in hydrogen (AuAg-MgO-H) was very similar to that before the reduction process. However, a significant increase in selectivity to propene was observed, indicating the generation of acidity as a result of hydrogen treatment of the sample. The same behaviour was observed after hydrogen treatment of monometallic sample (Au-MgO-H) indicating that the increase in acidity was not specific for the reduction of silver doped sample.

Summing up, introduction of silver to gold containing catalysts increased the acidity of the materials based on MgO and ZnO and decreased the acidity of niobia based materials. As concerns Lewis acid-

base pairs, they dominated on Au-Nb_2O_5 and AuAg-Nb_2O_5. Basic/redox activity evidenced by acetone selectivity for similar 2-propanol conversion degrees (16% on AuAg-ZnO; 18% on AuAg-MgO and 25% on AuAg-Nb_2O_5) followed the sequence:

AuAg-MgO > AuAg-ZnO > AuAg-Nb_2O_5.

3.4. The state of Au and Ag on the catalysts surface

The state of gold and silver in the catalysts prepared was studied by XRD, UV–vis, XPS and TEM techniques.

3.4.1. XRD

XRD patterns were examined to detect the presence of gold (Au^0) and silver (Ag_2O, Ag^0) phases in the catalysts. In the XRD pattern of Au-MgO (Fig. 1A), the peaks characteristic of metallic gold (2θ = 38.4, 44.5 and 64.8°) [20,21] were well visible, whereas for Au-Nb_2O_5 and Au-ZnO only the low intensity peak at *ca.* 44.5° appeared. Similarly, the reflections from silver phases were detected in the XRD patterns only for Ag-MgO (2θ = 38.3°, 44.5° and 64.6° from metallic Ag and 2θ = 32.3° from Ag_2O) [22]. The wide and weak reflections from metallic gold and silver phases in the XRD patterns of monometallic catalysts supported on ZnO and Nb_2O_5 (Fig. 1B, C) can be a result of a very good dispersion of small metal crystallites and/or the presence of silver oxide (the reflections from silver oxide can be overlapped with the XRD pattern of the support). For bimetallic AuAg-MgO and AuAg-ZnO reflections at 2θ = 38.5°, 44.4° and 64.9° were detected. However, as crystalline gold and silver have the same face centred cubic structures, it is difficult to assign these reflections to metallic gold, metallic silver or Au-Ag alloy phases [23,24].

3.4.2. UV–vis

UV-vis spectroscopy was used as a complementary technique to identify the state of the metals and alloy formation in the materials. In all UV–vis spectra of gold catalysts (Au-MgO, Au-ZnO and Au-Nb_2O_5) (Fig. 2), an absorption band at ca. 530–540 nm was observed. According to literature, this band was assigned to the surface plasmon resonance (SPR) band of metallic gold nanoparticles [24]. For bimetallic AuAg-Nb_2O_5 the position of this band was almost the same (537 nm) as for Au-Nb_2O_5. Interestingly, one can notice a red-shift of the band from metallic gold in the spectrum of AuAg-ZnO (543 nm) in comparison to its position in the spectrum of Au-ZnO (533 nm). Taking into account that the position of the band is sensitive to the size of gold nanoparticles [25], this shift suggests the presence of larger metal crystallites in AuAg-ZnO than in Au-ZnO. The formation of Au-Ag alloy after silver addition to gold was observed only for the bimetallic AuAg-MgO sample. As shown in Fig. 2, the position of the SPR band in the UV–vis spectrum was blue shifted from 528 nm for Au-MgO to 506 nm for AuAg-MgO. The shift observed is a result of Au-Ag interactions towards alloy formation. It is important to note that the low-intensity band at ca. 400 nm, typical of spherical silver nanoparticles [26,27], was observed only in UV–vis spectrum for Ag-MgO sample.

The spectra of all the catalysts supported on zinc and niobium oxides showed a very intense band between 200 nm and 380 nm coming from charge transfer in ZnO and Nb_2O_5. The UV–vis spectrum of Nb_2O_5 is typical of amorphous niobia [28]. The bands at *ca.* 220 nm and the broad band in the range 250–350 nm (with a maximum at *ca.* 280 nm) are characteristic of tetrahedral and octahedral Nb(V) species, respectively [29]. After metals incorporation on Nb_2O_5, one broad band attributed to the charge transfer transitions from O^{2-} to Nb^{5+} was observed in the spectra of catalysts. It suggests structural changes which were also postulated on the basis of textural parameters (Table 1).

It is known that the reduction process influences the formation and properties of Au-Ag alloy on the surface of catalysts by the enrichment of the alloy in silver [17,24,30,31]. That is why, in the next step of our study, the bimetallic catalysts were treated with hydrogen at 673 K, i.e., in the conditions used for activation before the catalytic oxidation of

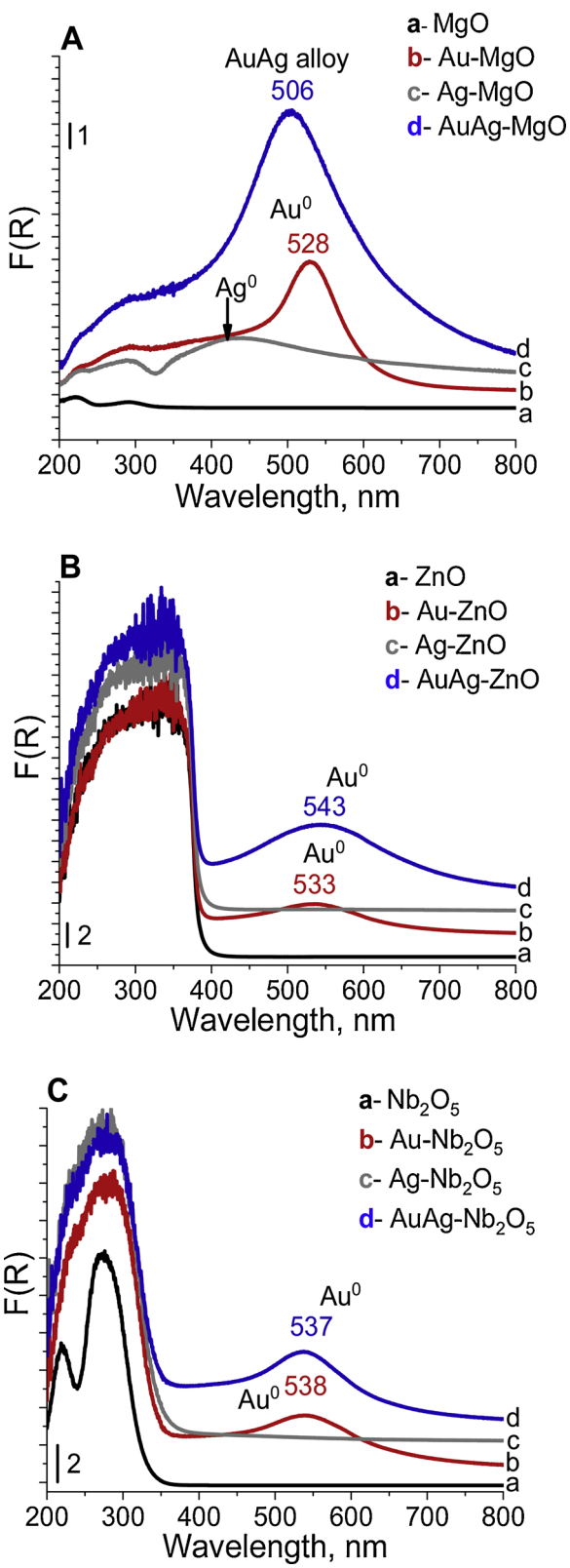

Fig. 2. UV–vis spectra of metal oxides before and after noble metals deposition and calcination: MgO (A), ZnO (B) and Nb_2O_5 (C).

octanol. The UV–vis spectra shown in Fig. 3 clearly revealed the effect of reduction treatment. A significant blue-shift of SPR band was observed for reduced bimetallic samples in comparison to the calcined samples (Table 4). The large blue-shift of the SPR band observed for AuAg-Nb_2O_5-H and AuAg-ZnO-H after hydrogen treatment (53 and

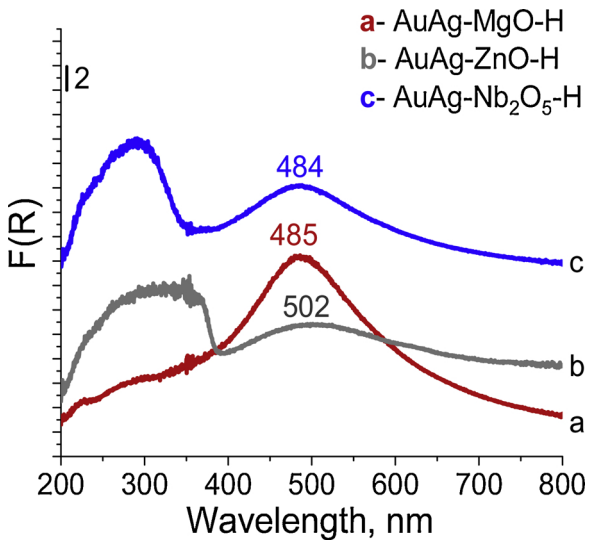

Fig. 3. UV–vis spectra of bimetallic catalysts after reduction treatment (-H).

Table 4
Wavelength of SPR bands in the UV–vis spectra of bimetallic catalysts.

Preactivation	Catalyst		
	AuAg-MgO [nm]	AuAg-ZnO [nm]	AuAg-Nb_2O_5 [nm]
Fresh catalyst after calcination	506	543	537
Reduced catalysts -H	485	502	484

41 nm, respectively) indicated the formation of Au-Ag alloy rich in silver on the surface of both catalysts. Much smaller blue-shift (from 506 to 485 nm, i.e., 21 nm) was found for AuAg-MgO-H. However, for this sample the formation of alloy was identified already in the untreated fresh sample after calcination. This suggests that additional silver atoms were alloyed with gold on the surface of AuAg-MgO during the reduction process (a shift by 43 nm relative to its position for Au-MgO). Finally, the results indicated the formation of Au-Ag alloy with a similar silver content in all bimetallic materials thermally treated with hydrogen.

3.4.3. XPS

XPS was applied to investigate the electronic state of gold in selected monometallic catalysts (the most active catalysts among those on the same support). The photo-electron spectra of Au-MgO-D, Au-ZnO-D and Au-Nb_2O_5-D are shown in Fig. S3. The region characteristic of gold species (spin orbital $Au4f_{5/2}$) is overlapped with that of Mg2s and Zn3p. Therefore, the oxidation state of gold was determined on the basis of $Au4f_{7/2}$ component. For all catalysts studied the binding energy (BE) of Au $4f_{7/2}$ was much lower (ca. 82.7–83.1 eV) than that of Au^0 of bulk metal (84.0 eV) [32]. The negative shift of binding energy has also been observed earlier for Au-TiO_2 and has been attributed to electron transfer from the support to the Au particle [33–35] leading to the generation of $(Au^0)^{\delta-}$ species. One can conclude the presence of negatively charged metallic gold particles on the surface of MgO, ZnO and Nb_2O_5. The lowest BE (82.7 eV) was observed for Au-MgO-D indicating the highest electron transfer from MgO support to gold particles. As a result, metallic gold on MgO had the largest negative charge among all samples studied. Besides metallic gold, also cationic gold was present in the catalysts (BE ~ 84.6–84.8 eV), but in much lower amount.

3.4.4. TEM

Transmission electron microscopy (TEM) was used to get information about the average particle size (Table 2) and particle size distribution of the metals loaded on ZnO, MgO and Nb_2O_5. Particle size distribution histograms and TEM images are shown in Fig. 4. It is clear that the average metal particle size depended on the type of the support, active phase composition (Au *vs*. AuAg) and hydrogen treatment. The largest gold crystallites (16.9 nm) and the broadest particles size distribution were found for Au-MgO. The gold particles loaded on ZnO and Nb_2O_5 were much smaller (*ca.* 3–5 nm) and with narrow size distribution. Similarly, the average size of metal particles on AuAg-MgO was much bigger (8.9 nm) than on AuAg-ZnO and AuAg-Nb_2O_5 (3.8 and 3.7 nm, respectively). It indicates that the effect of silver is also different depending on the support. The addition of silver limited aggregation of metal particles during calcination for AuAg-MgO (the size of crystallites was significantly decreased), and AuAg-Nb_2O_5, whereas for AuAg-ZnO an increase in the particle size was observed (a decrease in the number of metal particles with diameters in the range 1–2 nm from 55% to 5%). Again, the particle size distribution for AuAg-Nb_2O_5 and AuAg-ZnO catalysts was much narrower than for AuAg-MgO. It is worth noticing that average size of metal particles in mono- and bimetallic samples did not change under reaction conditions (cf. Fig. S4).

The hydrogen treatment of bimetallic AuAg-MgO and AuAg-ZnO led to an increase in the average size of metal particles (Fig. 5) indicating that the reduction process favours aggregation of metal particles as a result of Au-Ag alloy formation. A similar behaviour has been observed earlier for AuAg-SBA-15 and AuAg-Zn/SBA-15 catalysts [17]. After the reaction the average size of particles in AuAg-MgO-H and AuAg-ZnO-H did not change significantly (Fig. S4).

3.5. Oxidation of n-octanol

Oxidation of n-octanol was performed at a relatively low temperature (353 K) under atmospheric pressure using oxygen as oxidant, and without the use of base with the solvent, i.e., under very mild conditions, in line with the green chemistry principles. The results obtained are shown in Figs. 6–9.

3.5.1. Activity

The effect of the support nature, active phase (mono- vs bimetallic) and catalysts preactivation (dried or after thermal treatment in H_2) on the catalytic activity was studied. The bare supports (MgO, ZnO, Nb_2O_5) were inactive in this reaction. As shown in Fig. 6, in all cases alcohol conversion increased with run time, but the activity of mono- and bimetallic samples strongly depended on the acid-base properties of the support surface and on the type of thermal treatment. For dried gold catalysts the order of activity after 6 h of the reaction was: Au-MgO-D > Au-ZnO-D > > Au-Nb_2O_5-D. This order is consistent with the basicity of the supports determined on the basis of 2-propanol decomposition. The results obtained are in line with the earlier reports for Au/TiO_2 modified with MgO [6] showing a positive effect of an electron-donor additive (MgO) on electronic and catalytic properties of the supported gold. Interestingly, there is no relationship between the order of activity presented above and the gold NPs size shown in Fig. 4, as the average size of gold particles changed in the order: Au-MgO-D > > Au-Nb_2O_5-D > Au-ZnO-D. Similarly no relationship between the activity and gold NPs size was found for methanol oxidation [17,31,36,37]. Thus, the role of the support nature has to be considered concerning its influence on electronic properties of gold. For this purpose the intermediate electronegativity of metal oxides was calculated according to the Sanderson's equation [38,39]. Intermediate electronegativity of the supports (taking into account electronegativity from Pauling's scale) was as follows: 2.12 for MgO, 2.38 for ZnO, and 2.76 for Nb_2O_5. The electronegativity of gold is 2.54, i.e. higher than that of MgO and ZnO and lower than intermediate electronegativity of Nb_2O_5. The electronegativity of gold NPs higher than that of the support favours electron transfer from the support to gold NPs. Electrons are accumulated on faces of gold particles and therefore large gold NPs are useful for this purpose. Negatively charged gold particles $(Au^0)^{\delta-}$ are known as active

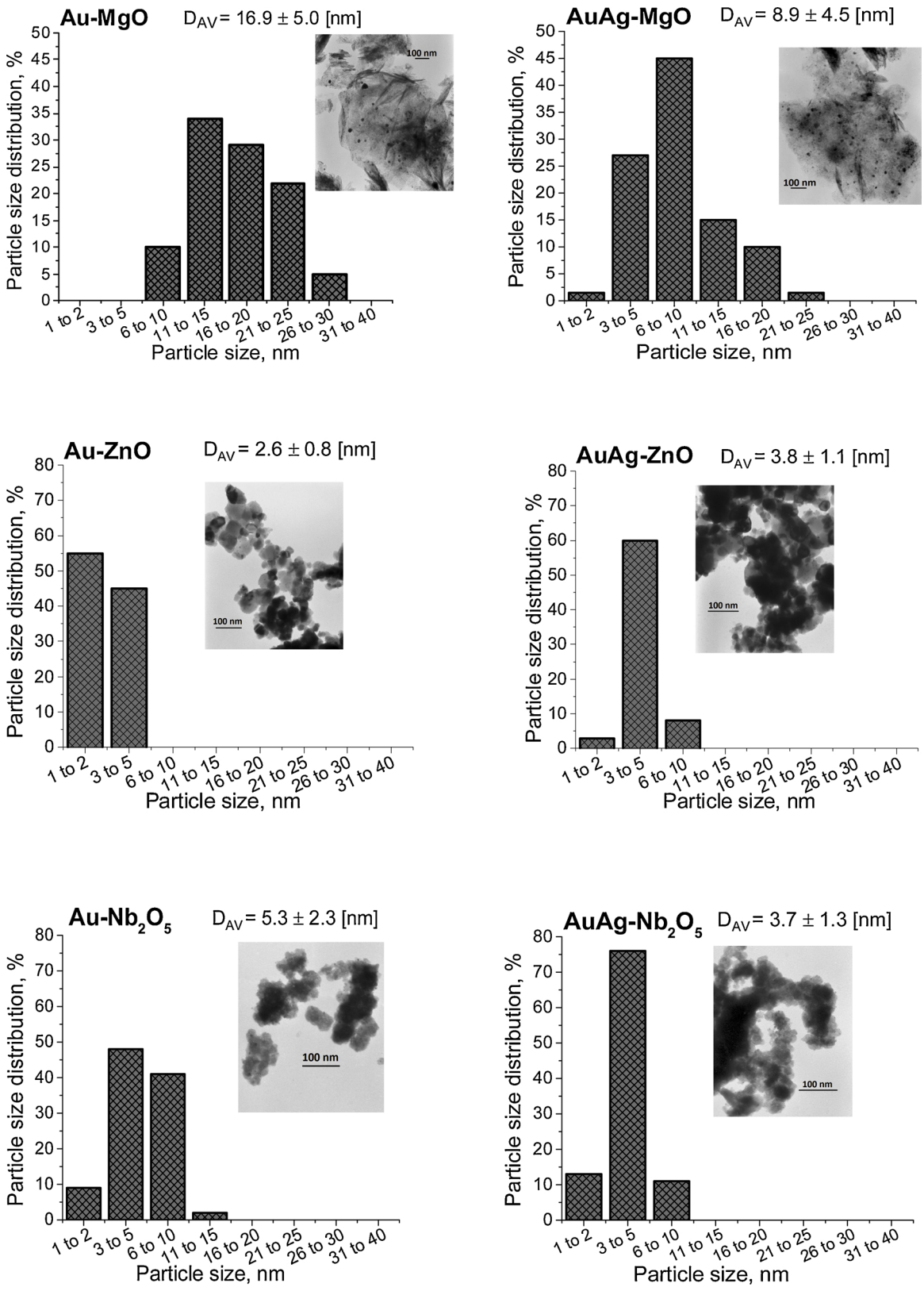

Fig. 4. Metal particle size distributions and TEM images of calcined catalysts.

species, e.g. in oxidation of methanol [17,31,36] and glycerol [40]. By contrast, intermediate electronegativity of Nb_2O_5 is higher than that of Au and therefore electron transfer can occur in the opposite way, from gold to support, making gold less negatively charged. The level of negative charge can be supported by the results of XPS study that showed the lowest BE for Au-MgO-D sample. Both kinds of electron transfer, from the support to gold and viceversa, enhance the oxidation activity by speeding up the steps of the redox cycle. Mobility of electrons can be determined by the difference in intermediate electronegativity between metal oxide (support) and gold NPs (active phase). It should be noted

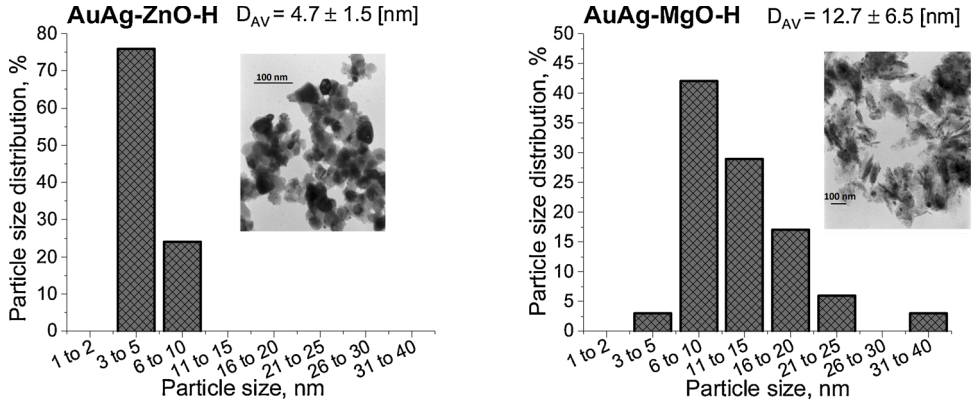

Fig. 5. Metal particle size distributions and TEM images of reduced bimetallic catalysts.

that the order of this difference (Δ) is in agreement with the sequence in n-octanol conversion: Au-MgO-D (Δ = -0.42) > Au-ZnO-D (Δ = -0.16) > > Au-Nb_2O_5-D (Δ = 0.22). Another parameter which is worth considering is the negative charge of oxygen in metal oxide, which is an indicator of support's basicity. The order of negative charge on oxygen (calculated according to Sanderson's equation) is in agreement with basicity estimated from 2-propanol test reaction and the activity in n-octanol oxidation: MgO (-0.341) > ZnO (-0.275) > Nb_2O_5 (-0.175).

The preactivation conditions also affected the activity of gold catalysts. The effect of catalysts pretreatment strongly depended on the support used for both gold and gold-silver catalysts. As concerns monometallic gold catalysts, the most significant influence of the conditions of thermal treatment was observed for Au-MgO (Fig. 6). The conversion of n-octanol on Au-MgO-D was the highest (65% after 6 h), but after pretreatment in hydrogen flow (Au-MgO-H) it was considerably lower. As shown by 2-propanol test reaction, pretreatment in hydrogen flow diminished the basicity of oxygen in MgO which resulted in lowering electron mobility, important in oxidation of n-octanol.

On the contrary, Au-ZnO samples showed smaller differences in activity depending on preactivation conditions, although the decrease in activity after hydrogen treatment was clearly seen. Both catalysts supported on Nb_2O_5 (Au-Nb_2O_5-D, Au-Nb_2O_5-H) showed the lowest activity from among the catalysts studied, which can be related to the acidic properties of the support [8] and the lowest electron mobility. Preactivation of Au-Nb_2O_5-D in hydrogen flow led to a slight decrease in activity (Fig. 6).

The order of activity of gold-silver catalysts on different supports was similar to that of monometallic gold catalysts, irrespectively of the preactivation conditions (MgO > ZnO > Nb_2O_5). A comparison of the activity of mono- and bimetallic gold catalysts supported on MgO and ZnO indicates that the addition of silver to gold decreased the activity in n-octanol oxidation for dried samples (Fig. 6). On the contrary, for the hydrogen pretreated AuAg-MgO-H and AuAg-ZnO-H the addition of silver increased n-octanol conversion on AuAg-MgO-H (26% vs. 32% after 6 h for Au-MgO-H and AuAg-MgO-H, respectively), while on AuAg-ZnO-H the conversion decreased (38% vs. 21% % after 6 h for Au-ZnO-H and AuAg-ZnO-H, respectively). It is noteworthy that a significantly higher alcohol conversion rate was obtained in the initial period of the reaction on AuAg-MgO-H than on Au-MgO-D, making AuAg-MgO-H sample the most active among the catalysts studied (Fig. 7). Another issue that should be considered is the role of the formation of Au-Ag alloy (as shown by UV–vis studies) on the catalysts activity. The content of silver in alloys was the same in all bimetallic samples but the metal particle sizes were significantly different, much

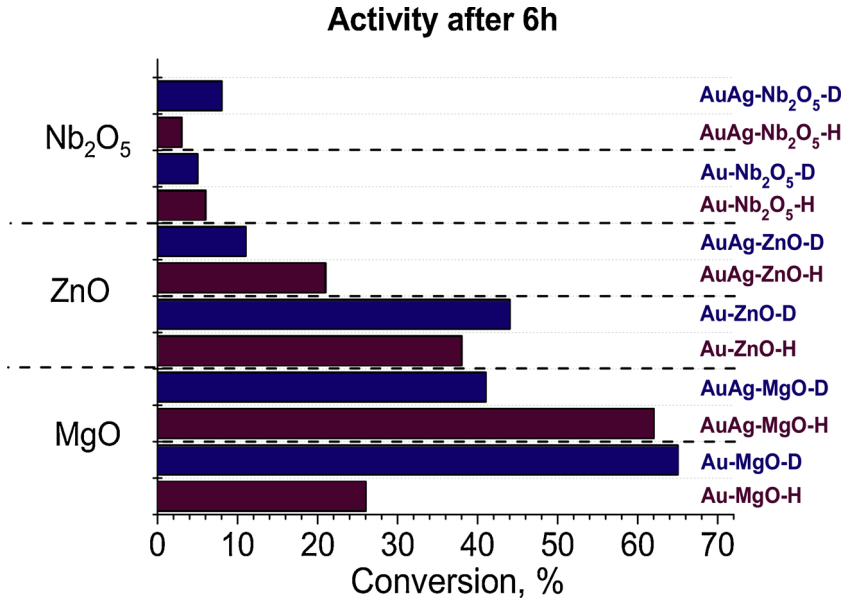

Fig. 6. Effect of catalyst composition and pretreatments on octanol conversion after 6 h reaction run.

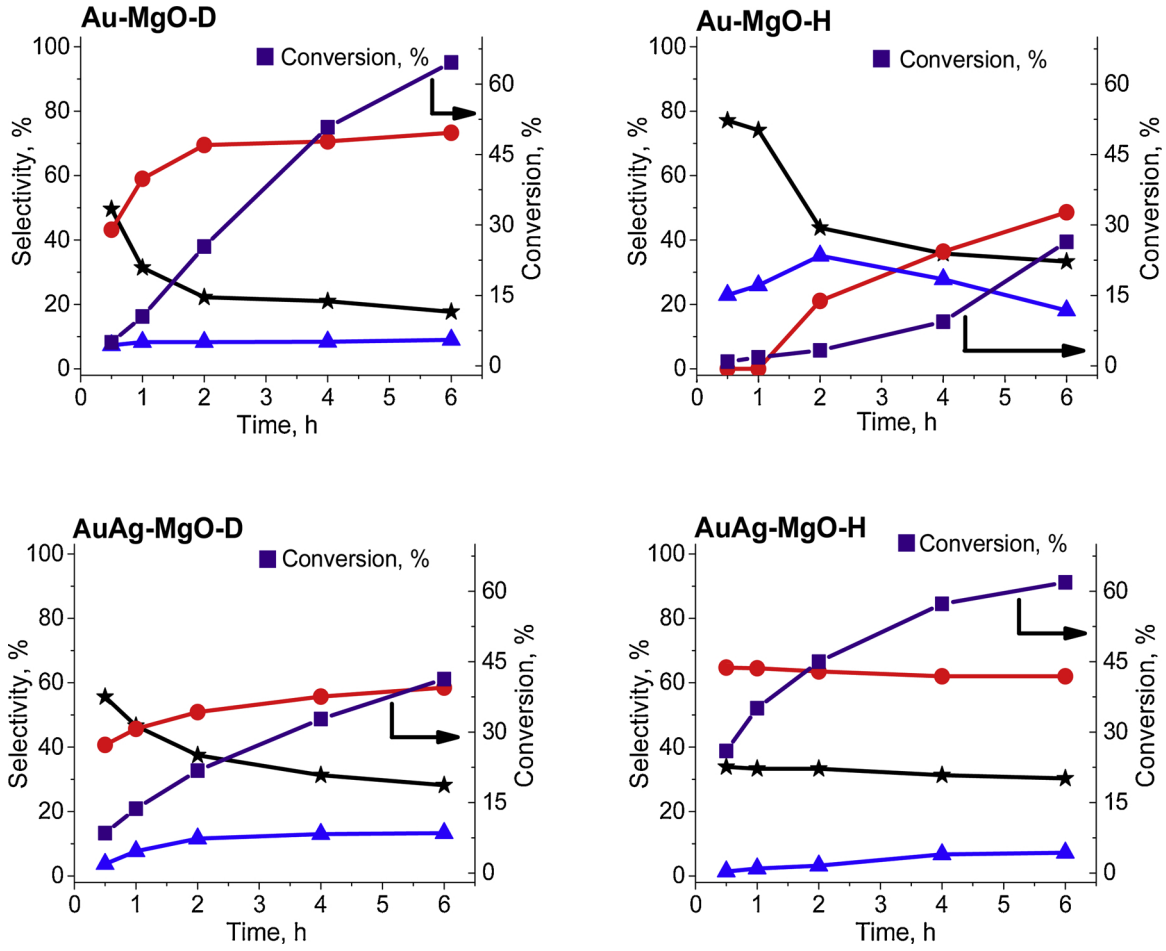

Fig. 7. Evolution of octanol conversion and products selectivity with reaction time in n-octanol oxidation over gold and gold-silver catalysts supported on MgO after drying (-D) or after reduction (-H). Symbols: aldehyde (stars), ester (circles) and acid (triangles).

larger on AuAg-MgO-H than on AuAg-ZnO-H. Larger metal particles favoured electron transfer from the support to gold (electrons are cumulated on crystal faces) and therefore AuAg-MgO-H (D_{AV} = 12.7 nm) was much more active than AuAg-MgO-D (D_{AV} = 8.9 nm) and AuAg-ZnO-H (D_{AV} = 4.7 nm). Similarly as observed for monometallic gold catalysts, the activity of AuAg-Nb_2O_5 samples was very low and the hydrogen pretreatment had little influence on alcohol conversion (Fig. 6).

To sum up, the combination of different properties of the catalysts (acidity – basicity, intermediate electronegativity of the supports, and metal particle size) determines the activity in n-octanol oxidation. However, the nature of the support (its intermediate electronegativity) plays the crucial role. Noble metals loaded on basic MgO exhibited the highest activity, whereas the lowest one was noted for all catalysts supported on acidic niobia.

3.5.2. *Catalysts selectivity*

For all the catalysts studied the main products of n-octanol oxidation were octanal and ester (octyl octanoate). Octanoic acid was only detected for MgO supported catalysts. However, the evolution of products distribution with run time was influenced by the type of the support, active phase (mono- vs bimetallic) and preactivation conditions (Figs. 7–9).

According to Haruta's group [8] the oxidation of n-octanol in a liquid phase on oxides supported gold starts from the oxidation of octanol to octanal on Au nanoparticles. The formation of the ester takes place by acetalization (the reaction of aldehyde with alcohol) to form the hemiacetal that is later oxidized to octyl octanoate. The ester can be also obtained from esterification of acid with alcohol. Hydration of octanal leads to the production of geminal diol, which can be further oxidized by oxygen to octanoic acid [41]. These different reaction pathways of n-octanol oxidation depend on the nature of active centres on the catalyst surface as shown in Scheme 1. The discussion on activity and selectivity, presented below takes into account the reaction pathways presented in this scheme.

For all catalysts based on MgO and Nb_2O_5 (with the only exception of bimetallic AuAg catalysts preactivated in hydrogen flow) octanal selectivity decreased and that of ester increased with the reaction time (Figs. 7 and 9), and therefore with the increase in n-octanol conversion. Thus, on the basis of the above-mentioned literature, it can be concluded that on these catalysts octyl octanoate could be formed via hemiacetal. The parallel oxidation of octanal to octanoic acid took place only on the catalysts supported on MgO. Thus, two competitive further transformations of octanal occur, i) acetalization and ii) oxidation to octanoic acid. The first requires the presence of high concentration of unconverted n-octanol (Scheme 1) and therefore if the conversion of alcohol is high, like on the catalysts based on MgO, the second reaction (oxidation to acid) takes place because the concentration of unreacted n-octanol is too low. The highest concentration of octanoic acid was observed for Au-MgO-H. For this catalyst, the acid formation decreased

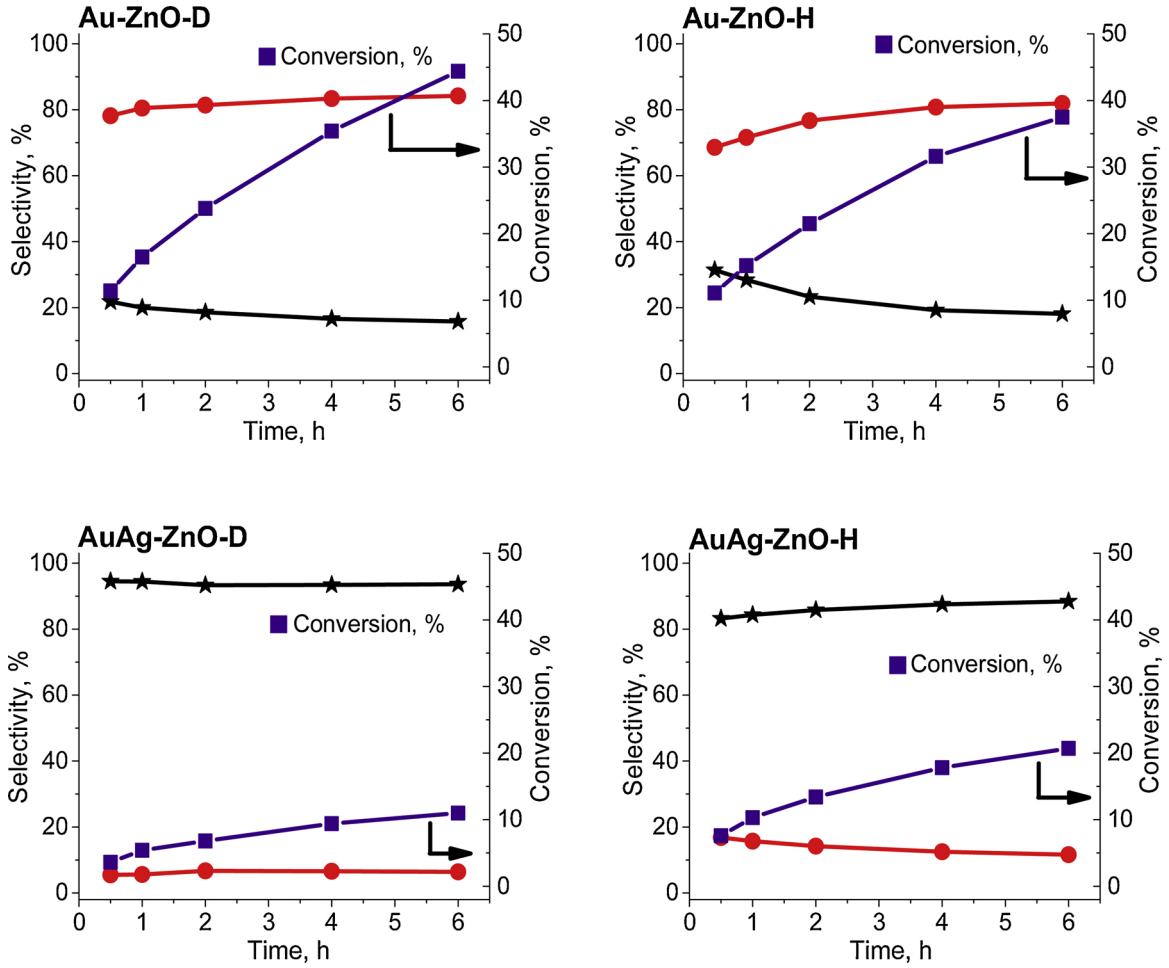

Fig. 8. Evolution of octanol conversion and products selectivity with reaction time in n-octanol oxidation over gold and gold-silver catalysts supported on ZnO after drying (-D) or after reduction (-H). Symbols as in Fig. 7.

with increasing reaction time, with a simultaneous increase in the ester formation. Thus, on this catalyst the ester was formed not only via acetalization but also by esterification of the acid with alcohol. Under the same reaction conditions octanoic acid was not produced over Nb_2O_5 supported catalysts, on which acetalization towards hemiacetal was responsible for the ester formation. However, it is noteworthy that the ester selectivity was lower, while that of aldehyde higher (ca. 50% and ca. 60–80% aldehyde selectivity for monometallic and bimetallic catalysts, respectively, after 6 h) than those observed over MgO supported catalysts. It indicates that on Nb_2O_5 supported catalysts the acetalization reaction took place to a lower extent. It has been reported [8] that octanal is formed on the surface of gold nanoparticles, but the ester on the border between the support and the metal loaded due to the acid-base catalysed reaction toward hemiacetal, which is further oxidized on the redox centres. Therefore, one can conclude that different acid-base properties of MgO (basicity) and Nb_2O_5 (acidity) were responsible for the differences in selectivity. Octanal was the only product over AuAg-Nb_2O_5-H. High selectivity to octanal was related to its desorption from the catalyst surface which was faster than the possible further reactions, i.e. acetalization or oxidation to octanoic acid.

Interestingly, on AuAg-MgO-H the selectivities to octanal, ester and acid were stable along the reaction time, although the conversion of alcohol increased continuously. Octyl octanoate was the main reaction product on this catalyst from the start of the reaction, in contrast to the selectivity evolution observed for all the other catalysts supported on MgO. It led to the conclusion that hydrogen treatment of this catalyst changed the properties of the metal-support perimeter enhancing acetalization reaction towards ester formation via oxidation of hemiacetal. The combination of redox centres (large gold particles loaded on electron-donor metal oxide) and the proper ratio between basic (from MgO) and acidic (generated after hydrogen treatment) sites is responsible for the high activity and stable products distribution observed.

For ZnO supported catalysts (dried and after reduction), a significant effect of metallic phase was found (Fig. 8). Over monometallic gold catalysts, octanyl octanoate was the main product and its selectivity slightly increased (reaching > 80% after 6 h), while that to octanal slightly decreased, with increasing conversion. In contrast, over bimetallic AuAg samples a high octanal selectivity (> 80% and > 90% for AuAg-ZnO-H and AuAg-ZnO-D, respectively) was obtained over the whole reaction time. The selectivity to the ester was low and no acid was detected in any case. The results obtained indicated than over AuAg-ZnO sample, neither the redox centres nor acid-base pairs were sufficient for further reaction of the aldehyde to the ester. It is important to note that after the reaction the plasmon band characteristic of AuAg alloy was observed in UV–vis spectra for bimetallic samples supported on ZnO were blue-shifted from 543 nm for AuAg-ZnO-D to 526 nm for AuAg-ZnO-DR and from 502 nm for AuAg-ZnO-H to 489 nm

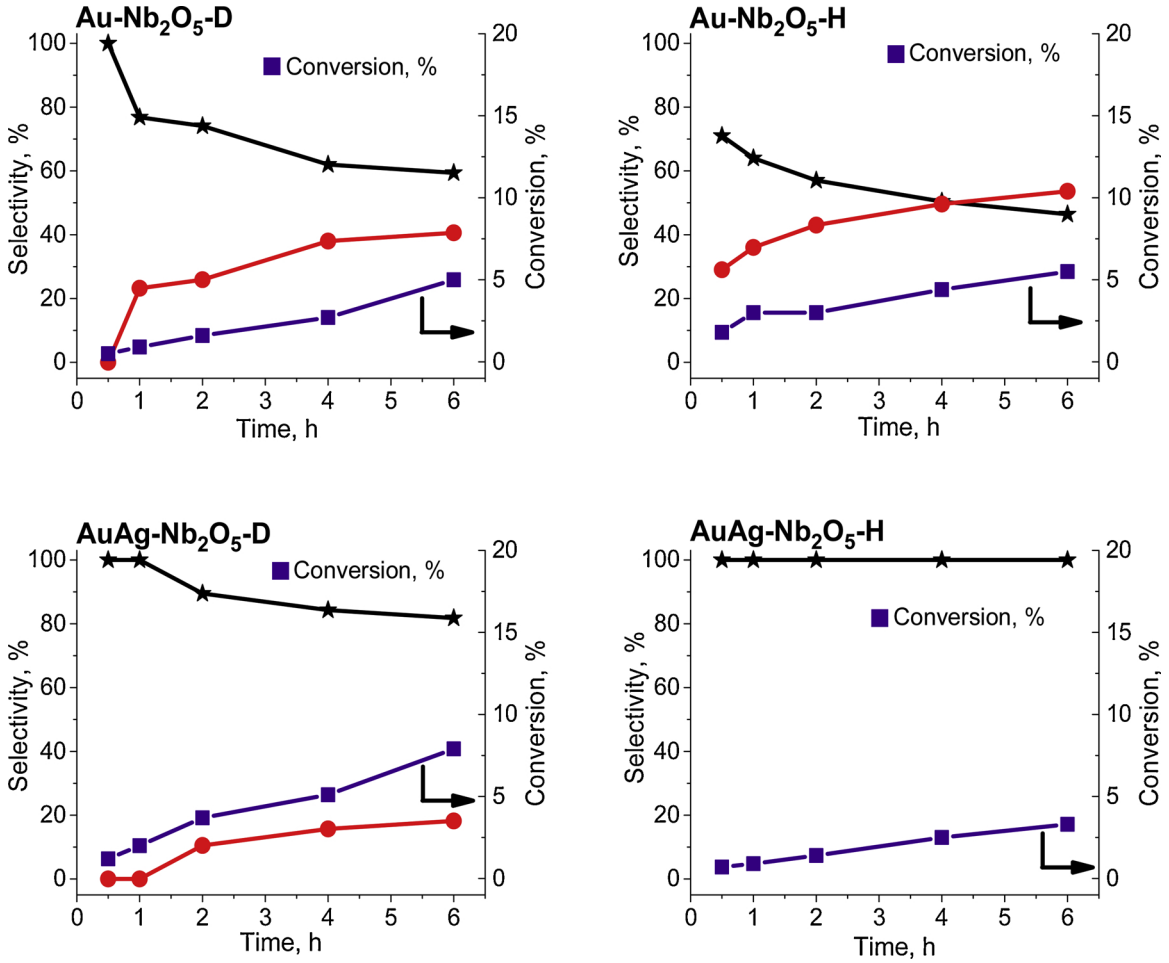

Fig. 9. Evolution of octanol conversion and products selectivity with reaction time in n-octanol oxidation over gold and gold-silver catalysts supported on Nb_2O_5 after drying (-D) or after reduction (-H). Symbols as in Fig. 7.

for AuAg-ZnO-HR (Fig. S5). This shift to lower wavelength indicates the enrichment of alloy in silver after the reaction. Such enrichment in Ag is understandable taking into account the effect of aldehyde present in the reaction products on the reduction of cationic silver, shown also in our earlier studies [30].

4. Conclusions

The use of three metal oxides (MgO, ZnO and Nb_2O_5) as supports for noble metals (Au, or Ag, or Au&Ag) led to different changes in their surface properties, showing some relationships between the nature of the support (basic MgO; acidic-basic ZnO and acidic Nb_2O_5) and metal active phase, as well as acidic-basic/redox properties of the catalysts prepared. Basic support (MgO) favoured the formation of larger metallic particles, both in mono- and bimetallic samples. Au-Ag alloys were formed in the latter, mainly after thermal activation in hydrogen flow. The content of silver in alloys in all bimetallic materials thermally treated with hydrogen did not depend on the support nature. The highest basic/redox properties were detected for AuAg-MgO. Such properties of the prepared materials influenced their activity and selectivity in n-octanol oxidation.

For high activity in n-octanol oxidation, high electron mobility

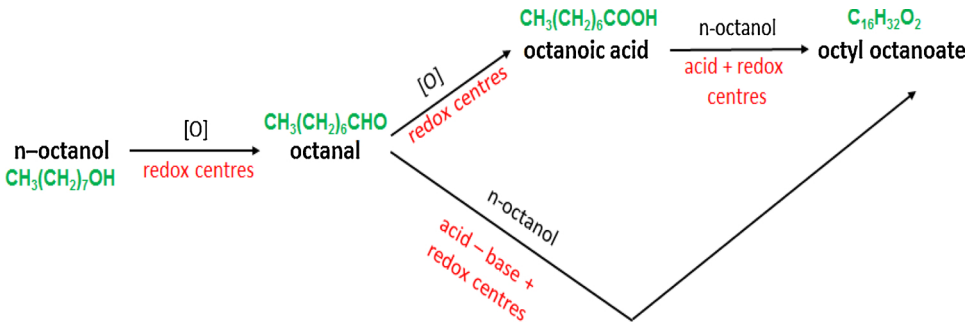

Scheme 1. Reaction pathways of oxidation of n-octanol.

between metal and basic support which plays a role of electron donor (MgO) was favoured. Electron donor properties of the support allow the accumulation of electrons on metallic gold particles, which are known to be important redox centres in oxidation processes. Gold played the role of redox active centres, whereas silver addition modified the acidic-basic properties of the catalytic system and in this way influenced the selectivity in n-octanol oxidation. It was evidenced that the proper ratio of acid-base properties and the presence of metallic redox centres were crucial for high activity and for controlling the selectivity of the reaction. The highest selectivity to the ester, reached already at the beginning of the reaction, was achieved on AuAg-MgO-H.

Declaration of Competing Interest

The authors declare that they have no known competing financial interests or personal relationships that could have appeared to influence the work reported in this paper.

Acknowledgements

Funding by National Science Centre in Poland (project N^{o} UMO-2018/29/B/ST5/00137), Erasmus + exchange programme and MINECO in Spain (project CTQ2017-86170-R) is acknowledged.

Appendix A. Supplementary data

Supplementary material related to this article can be found, in the online version, at doi:https://doi.org/10.1016/j.mcat.2019.110674.

References

[1] F. Boccuzzi, A. Chiorino, M. Manzoli, D. Andreeva, T. Tabakova, L. Ilieva, V. Iadakiev, Catal. Today 75 (1–4) (2002) 169–175.
[2] Y. Mizukoshi, T. Fujimoto, Y. Nagata, R. Oshima, Y. Maeda, J. Phys. Chem. B 104 (2000) 6028–6032.
[3] F. Ksar, L. Ramos, B. Keita, L. Nadjo, P. Beaunier, H. Remita, Chem. Mater. 21 (2009) 3677–3683.
[4] X. Huang, X. Wang, M. Tan, X. Zou, W. Ding, X. Lu, Appl. Catal. A: Gen. 467 (2013) 407–413.
[5] A. Villa, C. Campione, L. Prat, Catal. Lett. 115 (2007) 133–136.
[6] E. Kolobova, E. Pakrieva, L. Pascual, V. Cortés Corberán, N. Bogdanchikova, M. Farias, A. Pestryakov, Catal. Today 278 (2016) 104–112.
[7] S. Martínez-González, A. Gómez-Avilés, O. Martynyuk, A. Pestryakov, N. Bogdanchikova, V. Cortés Corberán, Catal. Today 227 (2014) 65–70.
[8] T. Ishida, Y. Ogihara, H. Ohashi, T. Akita, T. Honma, H. Oji, M. Haruta, ChemSusChem 5 (2012) 2243–2248.
[9] A. Rodríguez-Gómez, F. Platero, A. Caballero, G. Colón, Mol. Catal. 445 (2018) 142–151.
[10] Y. Kotolevich, E. Kolobova, A. Pestryakov, J.E. Cabrera Ortega, N. Bogdanchikova, V. Cortés Corberán, E. Khramov, Y. Zubavichus, R. Zanella, E. Pakrieva, Curr. Org. Synth. 14 (2017) 323–331.
[11] Y. Kotolevich, E. Kolobova, E. Khramov, M.H. Farias, Y. Zubavichus, H. Tiznado, S. Martinez-Gonzalez, V. Cortés Corberán, J.D. Mota-Morales, A. Pestryakov, N. Bogdanchikova, J. Mol. Catal. A: Chem. 427 (2017) 1–10.
[12] W. Gao, F. Li, H. Huo, Y. Yang, R. Li, Mol. Catal. 448 (2018) 63–70.
[13] D. Dutta, A. Phukan, D.K. Dutta, Mol. Catal. 451 (2018) 178–185.
[14] L. Saputra, T. Kojima, T. Hara, N. Ichikuni, S. Shimazu, Mol. Catal. 453 (2018) 132–138.
[15] A.J. Faqeeh, T.T. Ali, S.N. Basahel, K. Narasimharao, Mol. Catal. 456 (2018) 10–21.
[16] T. Chen, Z. Xu, L. Zhou, J. Qiu, M. Wang, J. Wang, Mol. Catal. 474 (2019) 110422.
[17] I. Kaskow, I. Sobczak, Ch.-M. Yang, M. Ziolek, Catal. Today (2019), https://doi.org/10.1016/j.cattod.2019.06.036.
[18] X. Liu, A. Wang, X. Yang, T. Zhang, C.-Y. Mou, D.-S. Su, J. Li, Chem. Mater. 21 (2009) 410–418.
[19] A. Gervasini, J. Fenyvesi, A. Auroux, Catal. Lett. 43 (1997) 219–228.
[20] D.I. Kondarides, X.E. Verykios, J. Catal. 158 (1996) 363–377.
[21] C. Kan, W. Cai, Z. Li, G. Fu, L. Zhang, Chem. Phys. Lett. 382 (2003) 318–324.
[22] Z.H. Dhoondia, H. Chakraborty, Nanomater. Nanotechnol. 2 (2012) 1–10.
[23] Z. Qu, G. Ke, Y. Wang, M. Liu, T. Jiang, J. Gao, Appl. Surf. Sci. 277 (2013) 293–301.
[24] A.-Q. Wang, J.-H. Liu, S.D. Lin, T.-S. Lin, C.-Y. Mou, J. Catal. 233 (2005) 186–197.
[25] Z. Zhong, S. Patskovskyy, P. Bouvrette, J.H.T. Luong, A. Gedanken, J. Phys. Chem. B 108 (2004) 4046–4052.
[26] L. Suber, I. Sondi, E. Matijević, D.V. Goia, J. Colloid Interface Sci. 288 (2005) 489–495.
[27] D. Chen, Z. Qu, S. Shen, X. Li, Y. Shi, Y. Wang, Q. Fu, J. Wu, Catal. Today 175 (2011) 338–345.
[28] D. Prasetyoko, Z. Ramli, S. Endud, H. Nur, Mat. Chem. Phys. 93 (2005) 443–449.
[29] T. Armaroli, G. Busca, C. Carlini, M. Giuttari, A.M.R. Galletti, G. Sbrana, J. Mol. Catal. A 151 (2000) 233–243.
[30] I. Sobczak, E. Dembowiak, J. Mol. Catal. A: Chem. 409 (2015) 137–148.
[31] I. Kaskow, A. Wojtaszek-Gurdak, I. Sobczak, Catal. Today (2019), https://doi.org/10.1016/j.cattod.2019.04.010.
[32] J.F. Moulder, W.F. Stickle, P.E. Sobol, K.D. Bomben, Handbook of X-ray Photoelectron Spectroscopy, Perkin–Elmer Corporation, Physical Electronics Division, Eden Prairie, (1992).
[33] S. Schimpf, M. Lucas, C. Mohr, U. Rodemerck, A. Bruckner, J. Radnik, H. Hofmeister, P. Claus, Catal. Today 72 (2002) 63–78.
[34] S. Arrii, F. Morfin, A.J. Renouprez, J.L. Rousset, J. Am. Chem. Soc. 126 (2004) 1199–1205.
[35] F.-W. Chang, H.-Y. Yu, L.S. Roselin, H.-C. Yang, T.-Ch. Ou, Appl. Catal. A 302 (2006) 157–167.
[36] L. Wolski, I. Sobczak, M. Ziolek, J. Catal. 354 (2017) 100–112.
[37] F.W. Chang, H.Y. Yu, L.S. Roselin, H.C. Yang, T.C. Ou, Appl. Catal. A Gen. 302 (2006) 157–167.
[38] R.T. Sanderson, Inorganic Chemistry, Reinhold, New York, 1967.
[39] R.T. Sanderson, J. Chem. Educ. 65 (1988) 112–118.
[40] P. Kaminski, M. Ziolek, J.A. van Bokhoven, RSC Adv. 7 (2017) 7801–7819.
[41] G. Jenzer, M.S. Schneider, R. Wandeler, T. Mallat, A. Baiker, J. Catal. 199 (2001) 141–148.